TEXTOR BUNDLE DIVERTOR

T. F. Yang, A. Wan, P. Gierszewski,
E. Rapperport, D. B. Montgomery

Plasma Fusion Center
Massachusetts Institute of Technology
Cambridge, Massachusetts 02139 USA

TABLE OF CONTENTS

ABSTRACT

This report presents a preliminary bundle divertor conceptual design for installation on the TEXTOR tokamak. An advanced cascade T-shaped coil configuration is used. This divertor design has the following important characteristics: (1) the current density in the conductor is less than 6 kAmp/cm^2, and the maximum field is less than 6 Tesla; (2) the divertor can be operated at steady-state either for copper or superconducting conductors; (3) the power consumption is about 7 MW for a normal conductor; (4) the divertor can be inserted into the existing geometry of TEXTOR; (5) the ripple on axis is only 0.3% and the mirror ratio is 2–4; (6) the stagnation axis is concave toward the plasma, therefore q_D is smaller, the acceptance angle is larger, and the efficiency may be better than the conventional circular coil design.

1

Neutral
beam
port

Advanced
bundle divertor

Bundle divertor
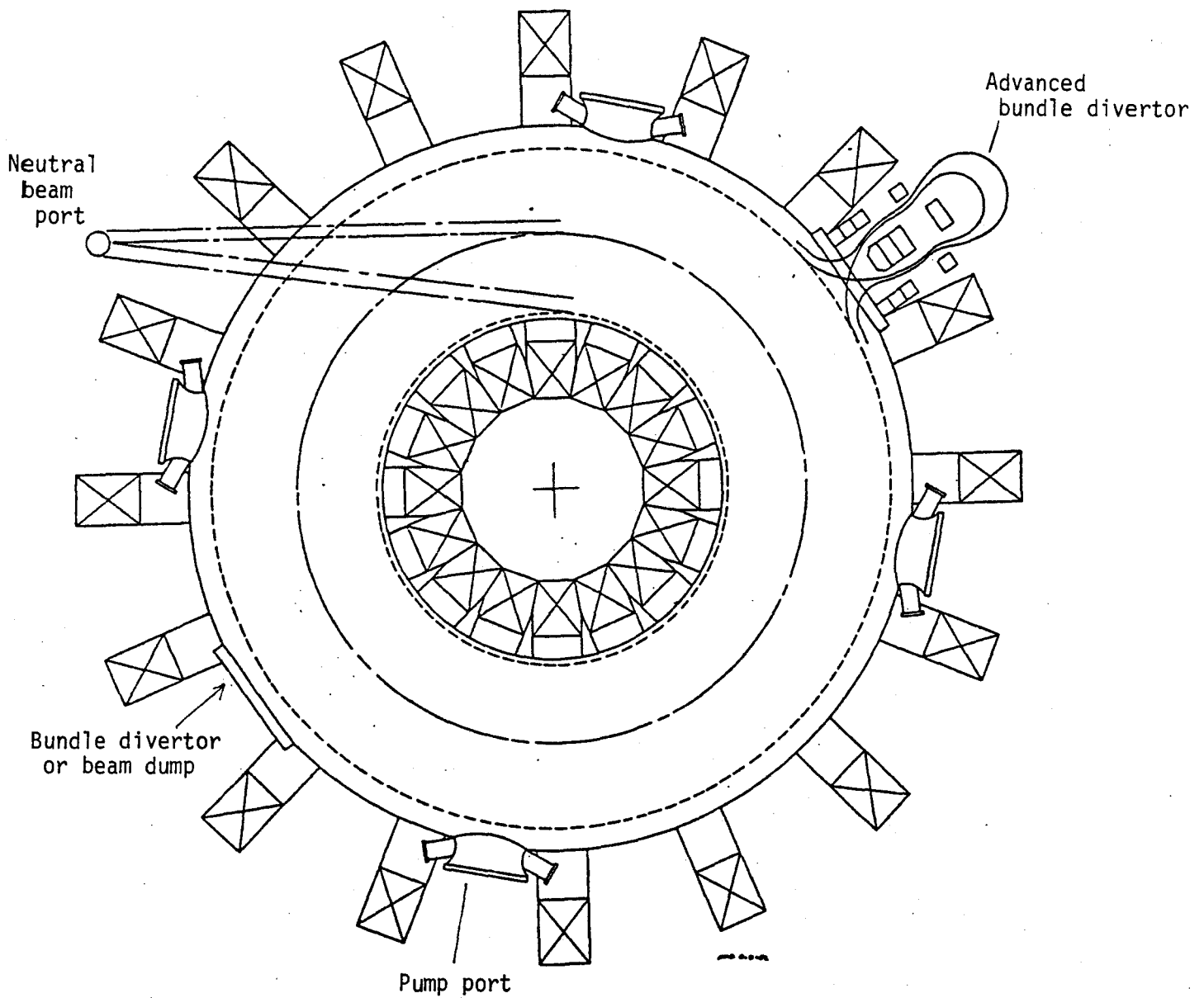or beam dump

Pump port

Fig. 1. Simplified layout of TEXTOR vacuum vessel with
the implementation of an advanced bundle divertor.
(not to exact scale)

1. INTRODUCTION

The overall objectives of TEXTOR [1], as is stated in the Technical Data I, are to evaluate the relative importance of the processes leading to the build-up of impurities in tokamaks and to the damage of the first wall under different operating conditions, to search for appropriate first wall materials, structures and temperatures that are optimized with respect to particle release and wall material behavior, and to develop and test methods to control the boundary. To accomplish the first objective a relatively controllable particle composite control mechanism is needed. TEXTOR has given the bundle divertor considerable thought as has been reported in the Divertor Workshop held at Culham Laboratory in England in 1977. There are provisions for two such divertors to be installed.

An optimization study [2] has shown that the performance of the bundle divertor is favored in a large device with a large aspect ratio among the existing tokamaks. TEXTOR is the best device for demonstrating a bundle divertor as can be seen from the following parameters:

<div align="center">

TEXTOR PARAMETERS

</div>

Major radius	$R = 1.75$ m
Minor radius	$a = 0.5$ m
Toroidal field (on axis)	$B_T = 2$ T
Plasma current	$I_p = 480$ kA at $q = 3$
Flux swing	$\Delta\phi > 4$ Vs
Inner temperature	$T_{max} = 600°$ C
Flat-top time	$t = 3$ sec

High poloidal beta and long pulse (5–10 seconds) may require effective impurity control methods of which none currently exist. The bundle divertor has proven at least 30% efficiency at less favorable conditions, hence this option should be vigorously investigated and supported. The simplified plane view of TEXTOR with the implementation of an advanced bundle divertor is shown in Fig. 1. Figures 2 and 3 show cross sectional and trimetric views. There are two large ports of 60 × 80 cm² each on the midplane of the vessel for housing the bundle divertor which are
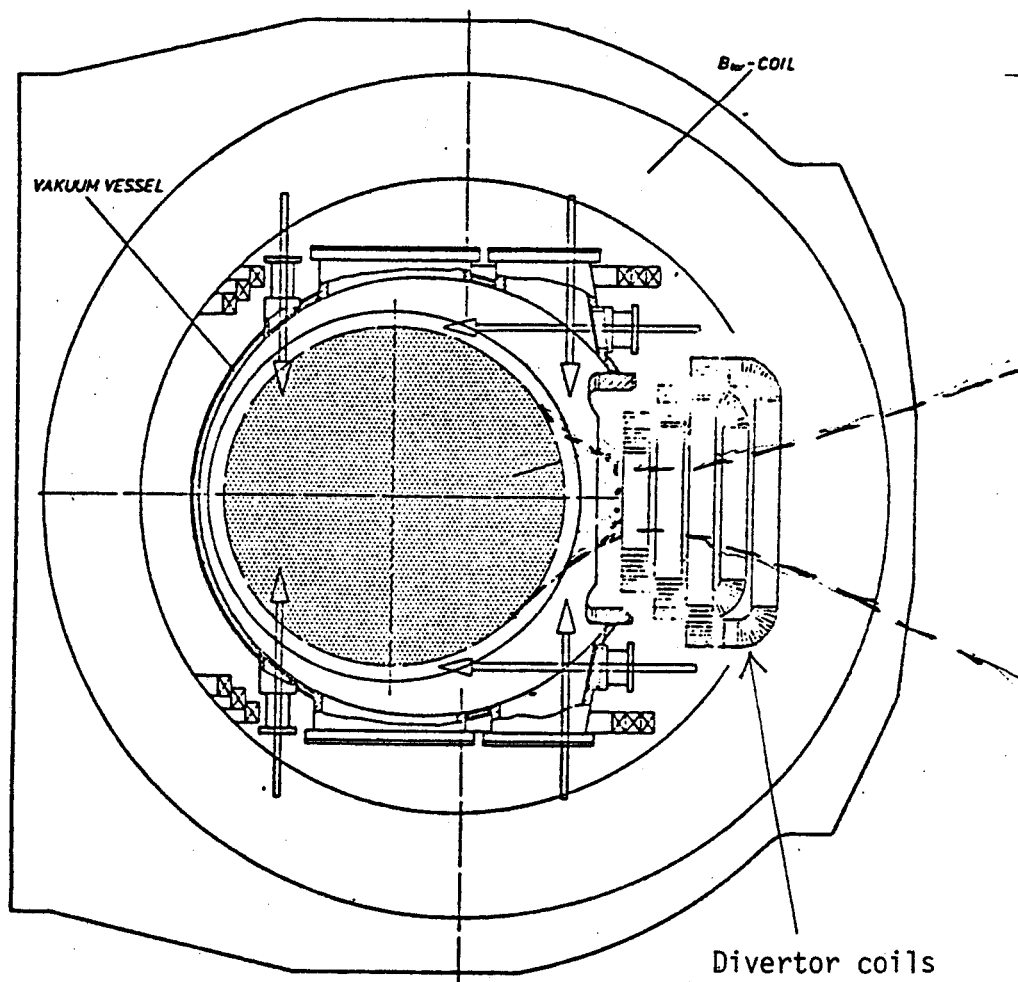
Fig. 2. Cross sectional view of the TEXTOR vacuum
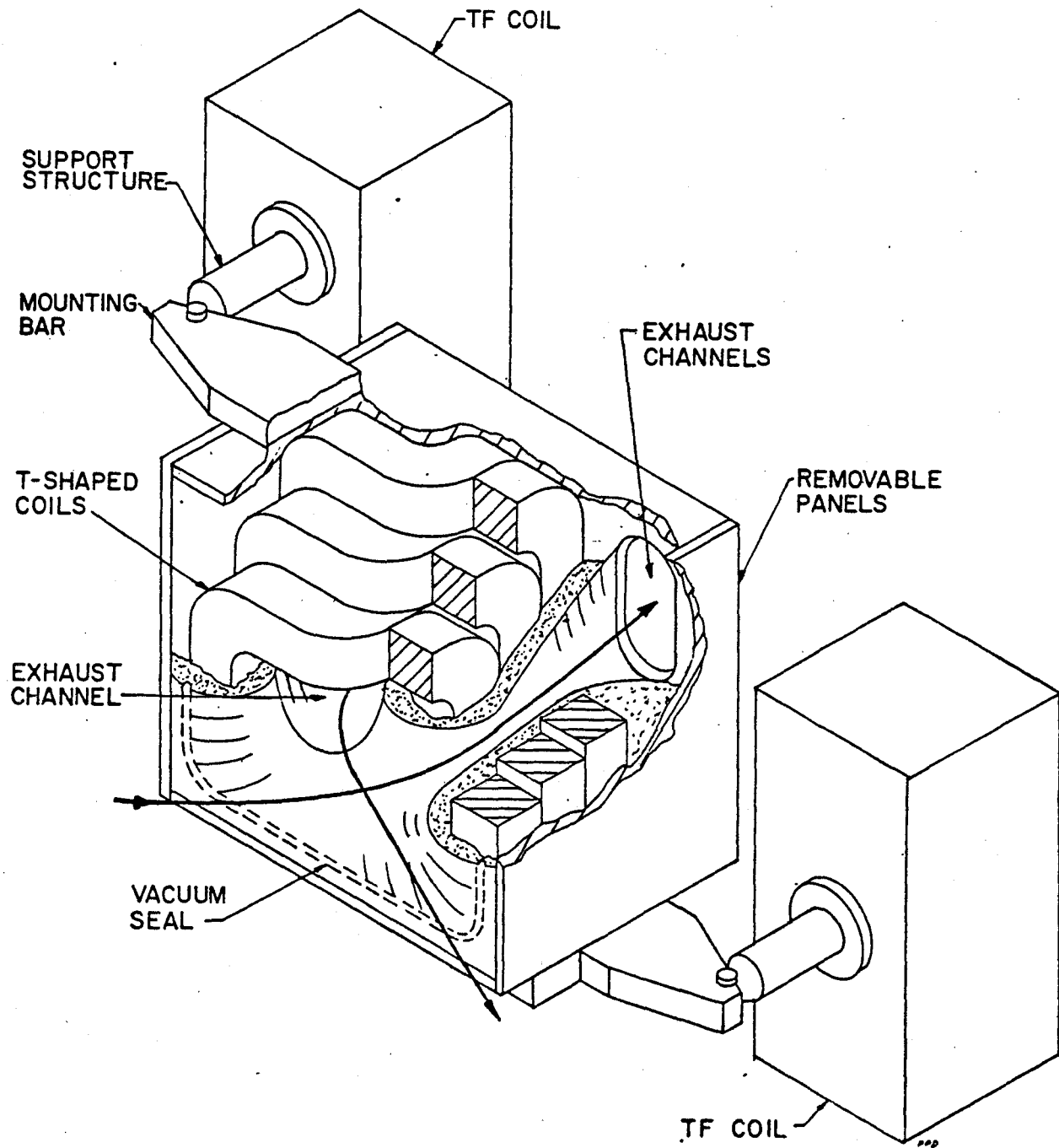vessel with divertor coils. (not to exact
scale)

4

Fig. 3. Illustration of engineering concepts of the
TEXTOR bundle divertor assembly.

5

currently being used as beam dumps. With these ports used for the bundle divertor, the beam dump could still fit into the large space between the vacuum vessel and the divertor. The bundle divertor shown here is a monolithic single unit construction which can be externally assembled and then inserted into the existing space. The divertor coil can be of either copper or superconducting conductors. In the case of a copper conductor the coils can be operated at steady state with 7 MW of power consumption.

Design parameters for three conventional circular coil bundle divertors have been obtained and compared with the new advanced configuration. The advantages of the new design are quite evident as is discussed in Section 3. Discussion of experimental observations is given in Section 4. In the Appendix the assessment of bundle divertors for reactors is discussed in general terms.

2. TEXTOR BUNDLE DIVERTOR

The magnetic configuration of a reference bundle divertor designed for TEXTOR is shown in Fig. 4. The diverted magnetic flux design was expanded for reducing the thermal load on the target and increasing the pumping efficiency. Expansion coils can be added or removed whenever necessary. Coil parameters are listed in Table 1 and the divertor coil configuration is illustrated by the trimetric views and projections in Fig. 5. The plane view and cross sectional view of this divertor as if installed on TEXTOR are shown in Figs. 1 and 2.

The divertor coils are cascade T-shaped. The width is limited by the space between the two adjacent TF coils, as the coils are designed to be inserted into the tokamak or pulled out as a single unit. As is discussed in the appendix, the cascade T-shaped coil configuration dramatically reduces the ripple and current density in the conductor and makes the size compact. The magnetic flux surfaces were found to be nonergodic and the particle confinement from the guiding center orbit study was also improved. Such a divertor was found to be feasible for a reactor. It has been shown that the divertor performs better on larger machines. This bundle divertor would not only provide for a long pulse impurity control experiment on TEXTOR, but the results will also be significant for reactors generally.
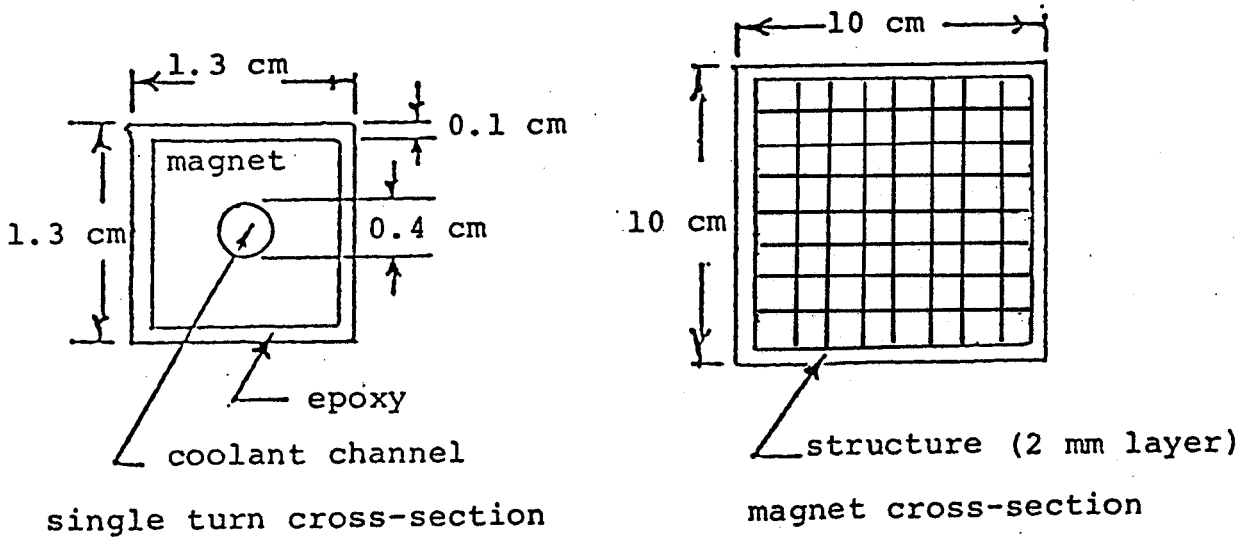
6

Table 1

Magnetic and Thermal Design Parameters for TEXTOR Bundle Divertor Reference Design

$B_o = 2.0$ T $B_{max} = 6.0$ T

$R_o = 175$ cm $I_d = 1.35$ MA·T

$a = 50$ cm $J_d = 4.5$ kA/cm^2

Normal Conductor Option for Steady State Operation

#Turns $= 64$

$p_{in} = 1.1$ MPa $p_{out} = 0.15$ MPa

$T_{in} = 27$ C $T_{out} = 57$ C

$w = 60$ kg/s $T_{copper} = 69$ C

$V_{in} = 13$ m/s   Power$= 6.5$ MW

Conductor Configuration

single turn cross-section

Total area/turn = 1.44 cm^2

Conductor area/turn = 1.084 cm^2

magnet cross-section

Epoxy area/turn = 0.23 cm^2

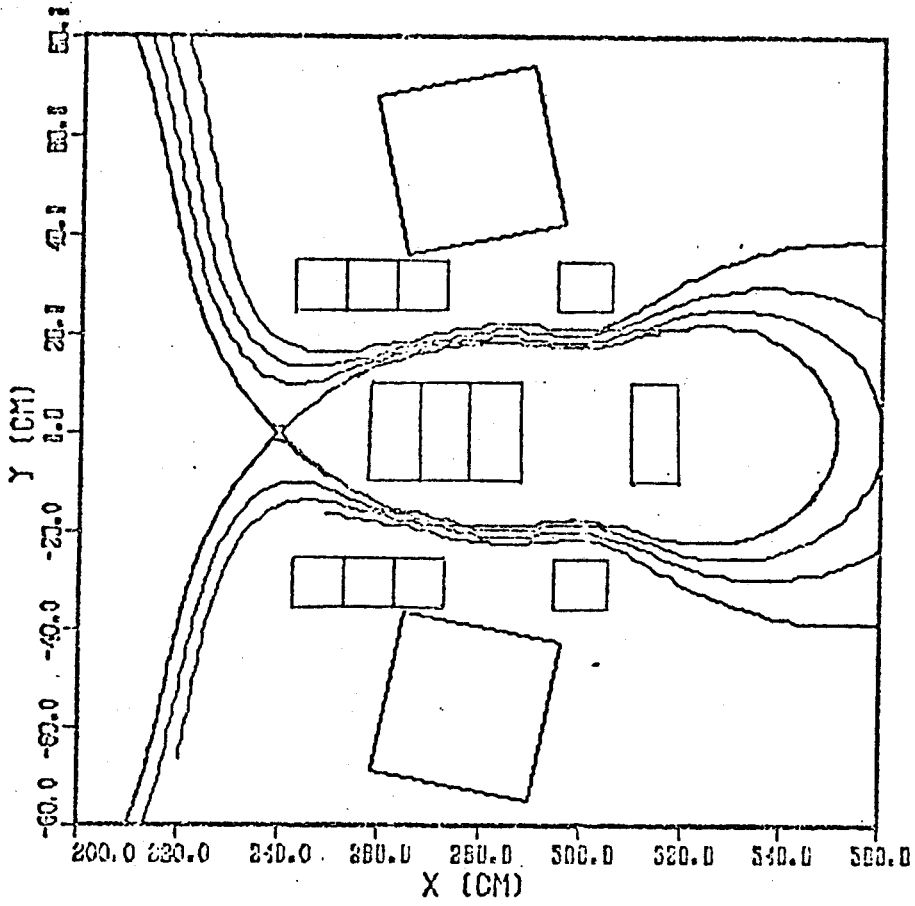Coolant area/turn = 0.126 cm^2

FLUX LINES

Fig. 4. The magnetic configuration for a reference
TEXTOR bundle divertor. The diverted flux
bundle is expanded.

8

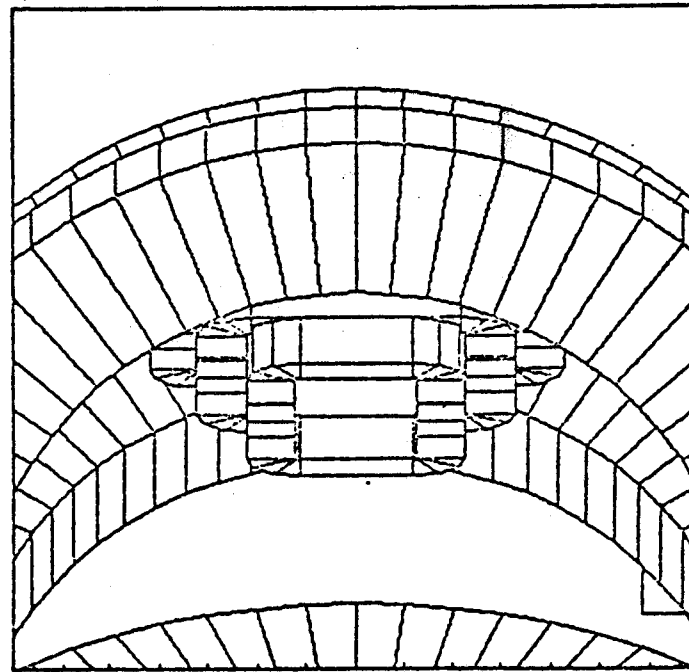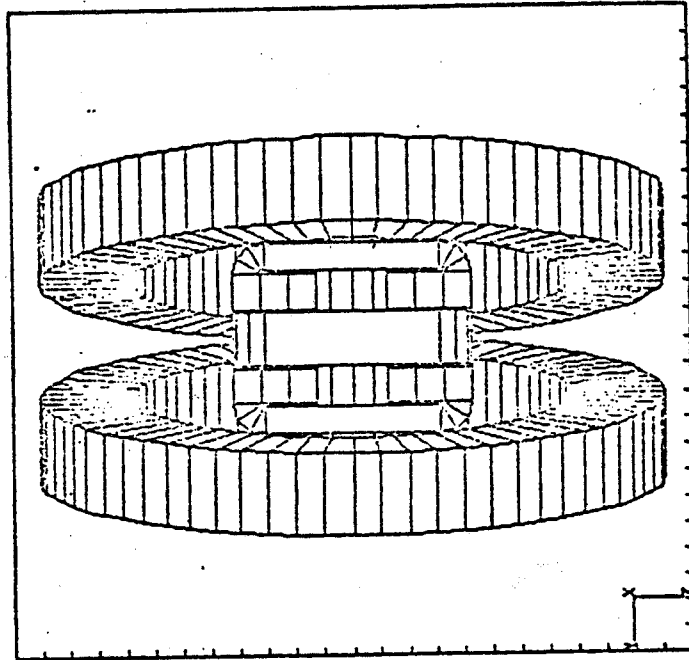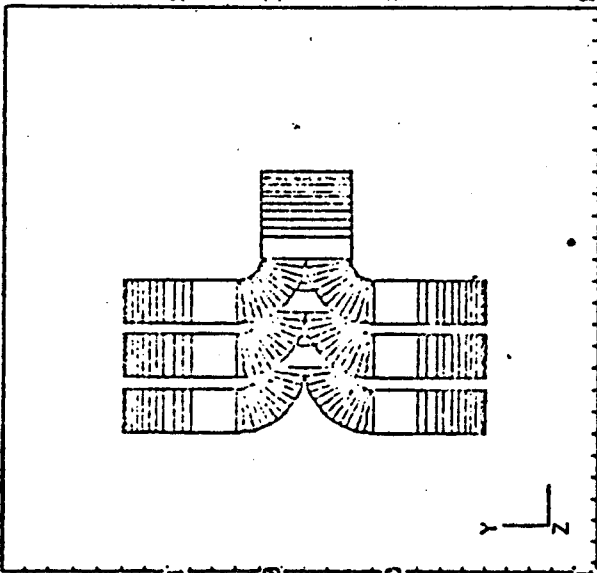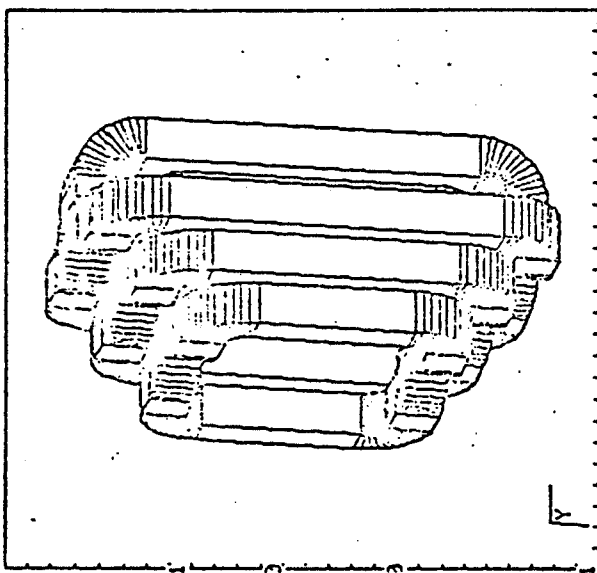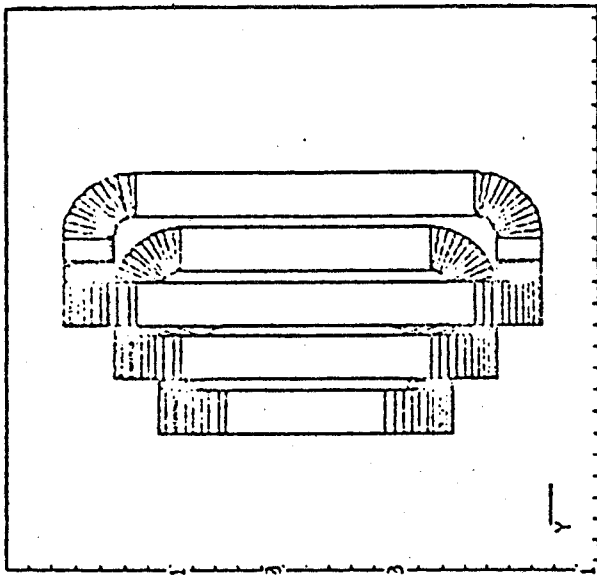Fig. 5. The projections and trimetric views of the divertor coils (top row) and the sectional view of the divertor inside two adjacent TF coils.

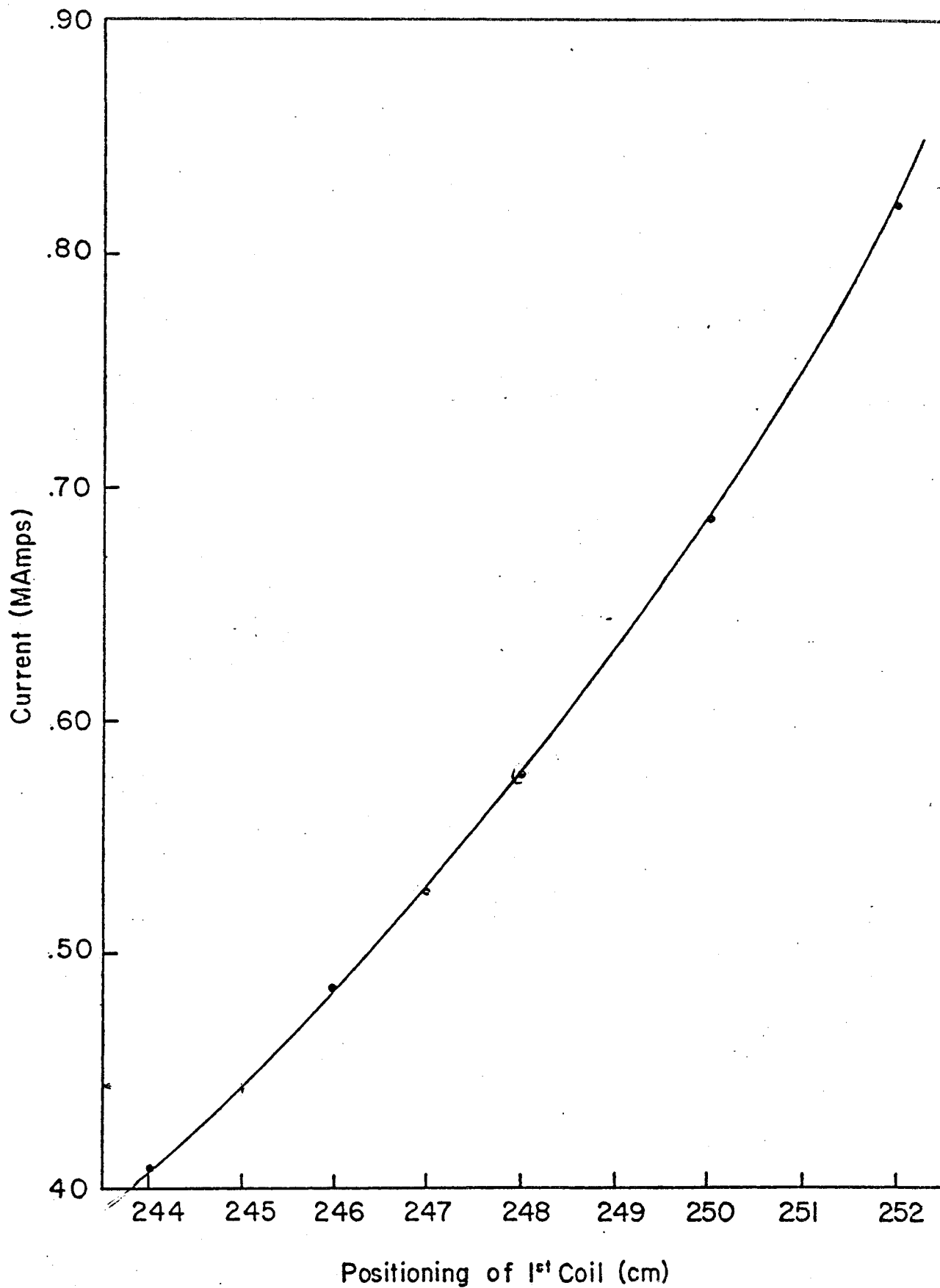# Current vs. Positioning of 1ˢᵗ Coil's Center Line

Fig. 6. Variation of divertor current with distance.

In order to select an appropriate dimension and location of the divertor coils within the constraints of the existing space, a variation study has been done. The current requirement in each coil as a function of radial distance is plotted in Fig. 6. The current design point is shown by a circle on the curve. The current and location may be readjusted as the design is refined.

The preliminary thermal characteristics are listed in Table 1. The thermal analysis was done using the same conductor as was used for the ISX-B bundle divertor. The conductor configuration is shown at the bottom of Table 1. The conductor of each turn has a cross section of 1.1 × 1.1 cm and the diameter of the cooling channel is 0.4 cm. There is a thickness of 1 mm insulation material (fiberglass tape and G-10 epoxy). The total number of turns is 384. The parameters listed are for steady state operation. The power consumption is less than 7 MW.

The engineering concept of the divertor is illustrated by the trimetric view shown in Fig. 3. The coil containment structure can be a monolithic unit; hence there is only one mechanical vacuum seal, as indicated by dashed lines on the front face, which will be bolted to the flange of the vessel. The passage for the diverted flux and plasma may be machined into the divertor housing. The top, bottom, side and back panels are all removable so that windings can slide into place and be available for improvement or repair. The divertor assembly is attached to the TF coils by two horizontal bars on the top and bottom. The bars are keyed to the divertor casing and attached to the TF coil structure by a cylindrical bearing. The net magnetic forces are transmitted to the TF coils; therefore the force balance for axisymmetric system is restored. This design will minimize the installation and disconnection time. The divertor assembly can be freed and extracted simply by lifting up and dropping down the holding bars.

3. COMPARISON OF THE CASCADE T-SHAPED AND CONVENTIONAL CIRCULAR DIVERTORS

For comparison purposes, three different magnetic divertor configurations for TEXTOR using a DITE MK-type [3,4] divertor have been calculated. The MK-type divertor has planar circular coils. The divertor performance and coil current are very sensitive to the size (radius of the circular coils) and angle α as shown in Fig. 7. The cross section of the coil is also shown in this figure. Comparative coil parameters, current, current densities, and ripple on axis are given in Table 2.

Table 2

Comparison of Advanced Bundle Divertors with MK-type
Bundle Divertor of Three Different Sizes

Divertor Type	X cm	Width cm	α deg	I MA·T	j amp/cm^2	Ripple %
MK	235	42.5	45°	1.04	8.32	.58
	240	42.5	45°	1.65	13.2	.87
	240	40	60°	1.35	12.0	.43
Advanced						
	240	30	T-shaped	1.32	4.4	.3
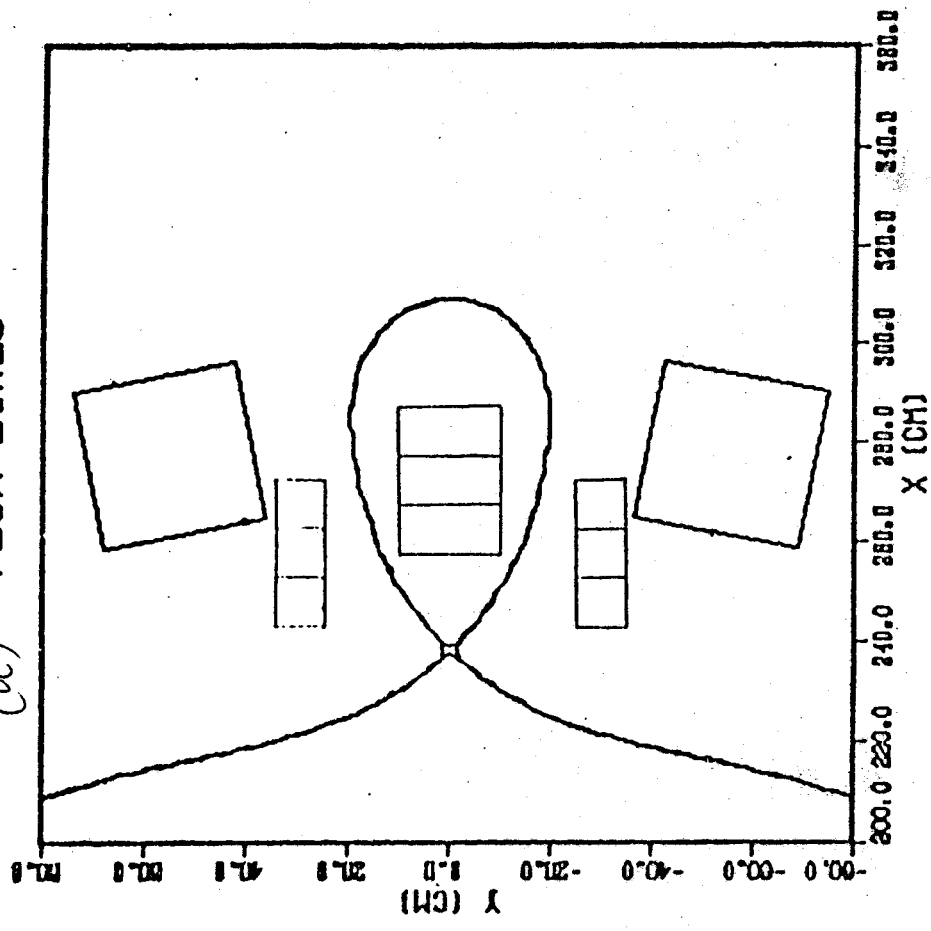
(b) FLUX LINES

(a) FLUX LINES

Fig. 7. Comparison of advanced cascade T-shaped TEXTOR bundle divertor (a) and MK-type planar circular TEXTOR divertor (b).
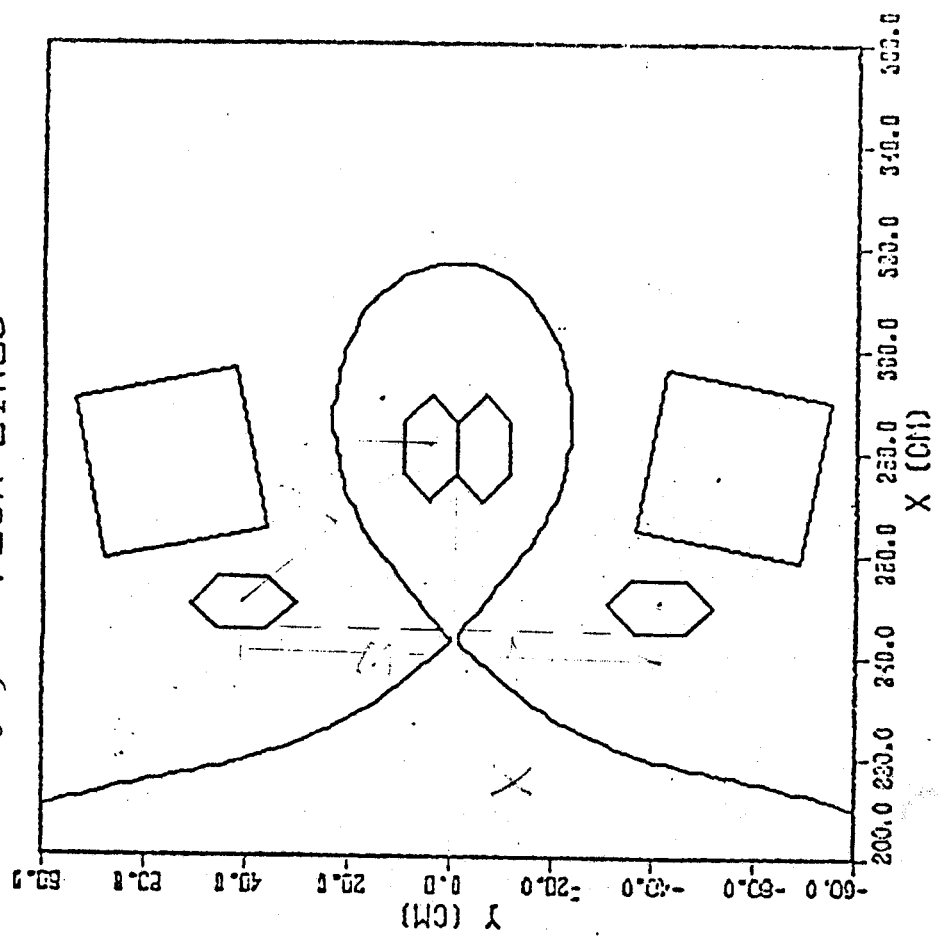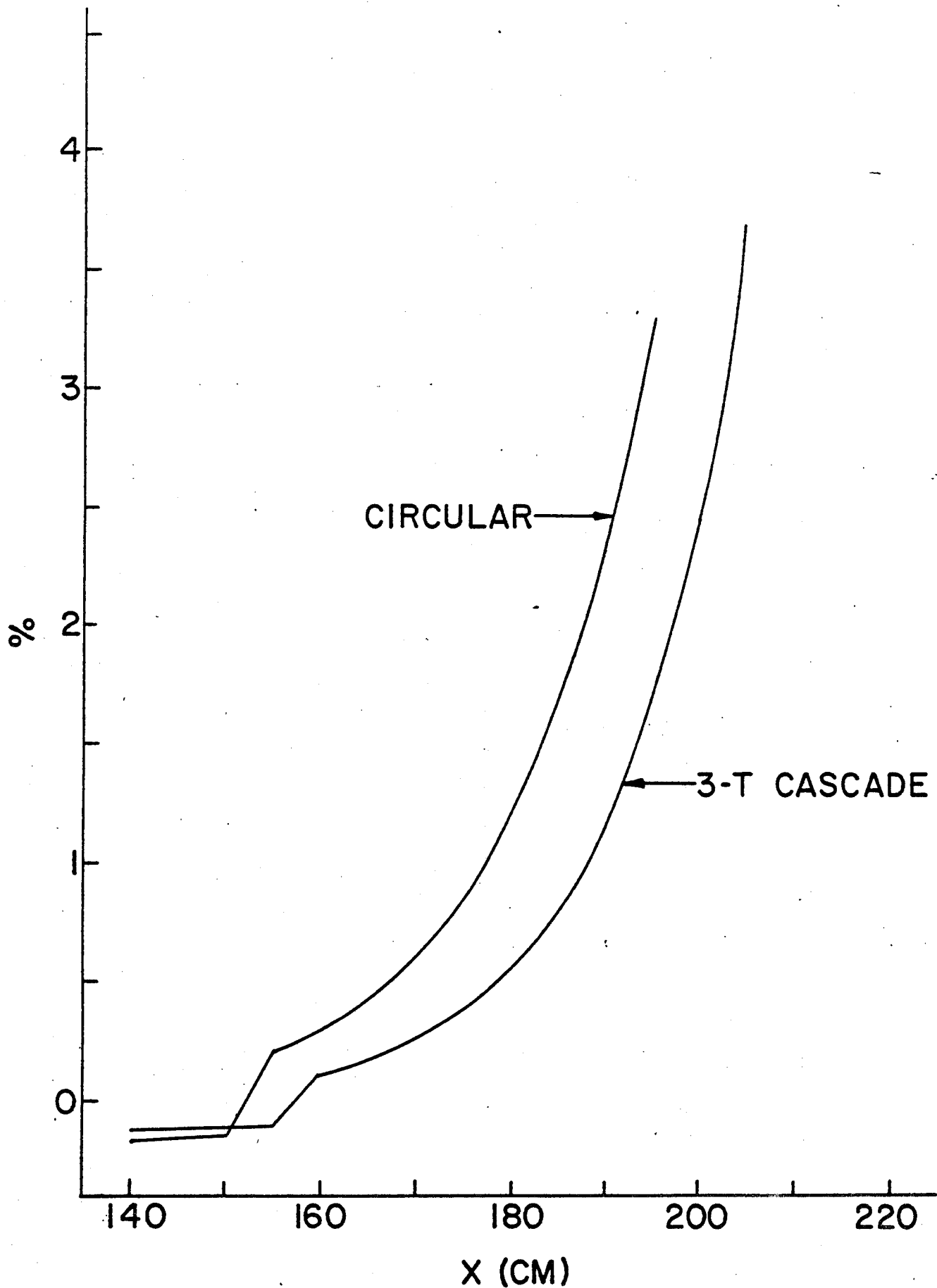
13

Fig. 8. Comparison of ripples for circular and cascade T-shaped divertors for TEXTOR.

14

The relative position of the divertor is given by X located on the front surface. The size is given by the width of the front opening. The current requirement for the advanced type divertor at the corresponding location W is given in the last column of Table 2. (The baseline divertor center is located further away at 245 cm.) Figure 8 compares the ripple MK-type and the advanced divertor.

All DITE MK-type divertors have to be placed very close to the plasma and have a larger size. The current density is at least twice as large as the case of the advanced type. The resistive heat for the MK-type is judged to be too large for long pulse operation. All the MK-type coils would interfere with the TF coils and the installation and service would be difficult. Due to space constraints the size of the MK-type divertor has to be reduced when it is moved away from the plasma, whereas for the advanced type the size can be fixed for various radial positions.

The advantages of the advanced type TEXTOR bundle divertor may now be summarized as follows:

(1)   The current density is low enough to permit steady operation at reasonable power consumption.

(2)   The ripple is low and flux surfaces are not ergodic. Thus the effect of the divertor on the confinement would be much less.

(3)   The null trace is straight vertically or concave toward the plasma and conforms better to the shape of the scrape-off layer; the diversion frequency, q_D, is thus smaller.

(4)   The successful experiment and data would be reactor significant.

4. ASSESSMENT OF DIVERTOR EXPERIMENTAL RESULTS

The sole experimental results available are from DITE. The data was taken with MK1A and MK1B divertors [3,4]. MK1B was a rebuilt version of MK1A. There are discrepancies in the results of the two experiments which will be explained later. However, some general conclusions may be given:

(1)   The separatrix acts as a limiter which determines the plasma current and density.

(2)   The particle exhaust efficiency is at least 30%. The efficiency will increase with density.

(3)   The parallel flow velocity is 0.4 times the speed of sound.

(4)   The impurity shielding efficiency is 35% and increases with density. The overall impurity reduction is typically 30% and higher for high z materials. There is a factor of 10 reduction in the X-ray anomaly factor on axis.

(5)   The bundle divertor has no adverse effect on the ion confinement from neutral beam injection.

(6)   The overall energy and particle confinement time was reduced by 30% when the plasma was operated at a safety factor less than 2 due to sawtooth instability.

To compare the MK1A and MK1B divertor experiments their parameters and characteristic conditons are given in Table 3. A summary of experimental results is given in Table 4. The electron temperature profile is shown in Fig. 9. The MK1A divertor was, under some circumstances, more efficient than MK1B. The explanation offered in Ref. 4 was that it was probably due to a higher proportion of supra-thermal electrons, and the presence of gross instabilities. In addition there are probably the following factors acting:

(1) q_D for MK1B is 7.4 and is larger than that of MK1A which is 6.5. In the meantime, the scrape-off layer is smaller due to the fact that the minor radius a_s is larger but the limiter radius is smaller. The combined effect will be larger cross field diffusion loss and higher radiation because it will take a longer time to divert the plasma into the divertor and less time to reach the limiter.

(2)   The MK1B was running at higher current, hence the vertical component of the magnetic field would be larger. The vertical excursion of the diverted field lines would be larger; thus some plasma might have struck the chamber wall before reaching the target.

(3)   A titanium coated vessel first wall and titanium limiter were used with the MK1B experiment instead of stainless vessel first wall surface and molybdenum limiters for MK1A. Titanium is an excellent gettering material with very high saturation dose. All the neutrals (both fast and slow) will be pumped by the large surface of the first wall which is more effective than bundle divertor because it encloses the plasma. This may explain why only 10% of aluminum impurity reached the hot plasma when the divertor was off. The combined impurity shielding efficiency may be only slightly better than 90% when the divertor was turned on, as one

16

Table 3

Parameters and Characteristic Conditions

Divertor	MkIA	MkIB	
Toroidal Field B_ϕ (T)	0.9	0.96	1.44
Major radius R_p (m)	1.17	1.17	1.17
Limiter material	molybdenum	titanium	titanium
Limiter minor radius a_L (m)	0.27	0.26	0.26
Separatrix minor radius a_s (m)	0.16	0.175	0.175
Mirror ratio M	4	3.6	3.6
Mean number of field line transits around torus per transit of divertor, $\bar{q}_D$	6.5	7.4	7.4
Usual working gas	hydrogen	deuterium	deuterium
Usual vacuum vessel wall condition	stainless steel	stainless steel covered by titanium	stainless steel covered by titanium
Plasma current I_p (kA)	45	55	85
Line of sight average density $\bar{n}_{eL}$ (m^{-3})	6×10^{18}	1.2×10^{19}	2×10^{19}
Central electron temperature Te(o) (eV)	300	450	550

Table 4

A Summary of Experimental Results

| Parameter	MkIA	MkIB	
density, $\bar{n}_{eL}$ (m^{-3})	~ 7 x 10^{18}	(6-8) x 10^{18}	1.2 x 10^{19}
particle exhaust: the fraction of the particle flux into the separatrix reaching the divertor	0.3 [10]	0.15	0.3
energy exhaust: the fraction of the conducted and convected power reaching the divertor	0.8 [5,7,8,10]	0.15	0.15
impurity screening: the fraction of incoming impurity flux reaching the divertor			
low Z:	0.5 [8,10]	0.25	0.35
high Z:	0.75 to 0.8 [8,10]	0.25	0.35
impurity line radiation from $r < a_s$, divertor on/divertor off			
low Z:	0.2 to 0.7 [6,7,12]	0.7 to 1.0	0.7 to 1.0
high Z:	0.02 to 0.3 [6,7,8]		0.7
radiated power, divertor on/divertor off	0.13 to 0.5 [5,7,8,12]	0.7 to 1.0	0.7 to 1.0
Z_{eff}, divertor on/divertor off	0.75 to 1.0 [5,6,7,8,10]		0.85 to 1.0
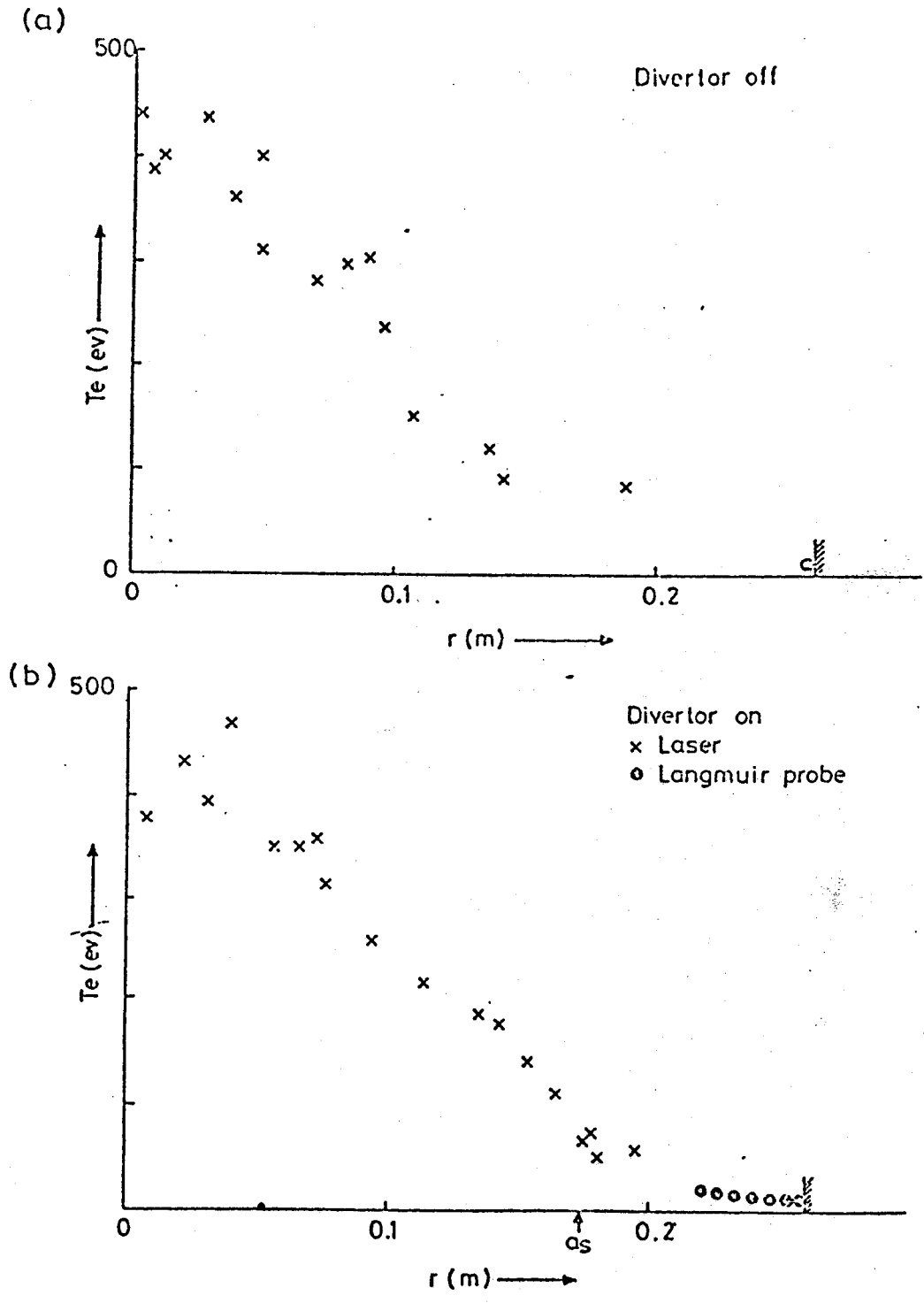
Fig. 9. Electron temperature profiles with divertor off and on.

19

would expect.

(4) The low shielding efficiency for neon might be explained as follows. The observed neon ion states $N_e VIII$ occur in the region where $T_e > 100$ eV. In the scrape-off layer $T_e \leq 50$ eV; therefore, the neon ionization rate is very low and the divertor would have very little effect. The gettering efficiency of neon titanium is near zero and neutral neon is likely to diffuse into the hot plasma. Therefore, to ensure the determination of true values of divertor efficiencies, testing of the bundle divertor would be made of nongettered first wall materials, higher density and higher temperature and/or injecting the impurities whose ion states would occur in low T_e in the scrape-off region.

5. SUMMARY

A preliminary design for an advanced type bundle divertor for TEXTOR has been designed. The divertor can be operated at steady state for a normal copper conductor. The efficiency is expected to be better than conventional planar circular coil divertors.

The experimental results from DITE prove that the overall efficiency for conventional divertors is at least 30% , which is already sufficient for reactors. The divertor was tested in an unfavorable condition, such as a small device, low field, low density and low temperature. The discrepancy between MK1A and MK1B may be due to the gettering wall material (titanium) and others used in the latter.

Since TEXTOR is a significantly large and high β tokamak, the divertor should be carefully designed and optimized in order to achieve the best results for particle control, and to provide significant information for reactors.

APPENDIX A

Bundle Divertor Assessment for a Reactor

A.1 ADVANTAGES

The bundle divertor has the following engineering advantages [5]:

1. The bundle divertor is a local appendix to the tokamak system; therefore, a major advantage is in it's modular replaceability and easy maintenance. Like the cascade divertor proposed for TEXTOR, it can be decoupled from the remainder of the tokamak system.

2. The bundle divertor chamber can be isolated from the main plasma chamber to a much greater extent than the poloidal divertor chamber. In some designs the target chamber is located completely outside the TF coils and the entire divertor can be replaced as a module. Consequently there is easier access for pumping ports and for replacement of the divertor plate. It should be possible to operate a bundle divertor with a higher density cooler plasma in the divertor chamber for a closer approximation to a gas target, since the throat in a bundle divertor can be longer and have a smaller cross sectional area than the throat in a poloidal divertor. The streaming jet action of the plasma should maintain a larger pressure gradient along the throat.

3. Substantial reductions may be achieved in the size of both the toroidal and poloidal field coil sets. With the space saved by eliminating the poloidal divertor, the height of the TF coils could be reduced to an inner bore of between 7 and 8 meters, reducing both coil material and stored magnetic energy. Since the poloidal field coils could then be placed closer to the plasma. While remaining outside the TF coil set, they would require less current for plasma shaping and therefore exert less out of plane force on the TF coils. The shape of the TF coils need not conform to the "constant tension" D shape.

4. The bundle divertor separatrix is fixed relative to the first wall and the divertor coils can be operated in steady state. The outer wall is therefore protected during start up, shut down, and disruptions. By way of contrast, the separatrix of a poloidal divertor with distant poloidal

field coils is sensitive to the distribution of plasma currents as well as fluctuations in coil currents and may be very hard to control.

A.2 A FEASIBLE BUNDLE DIVERTOR MODEL FOR POWER REACTORS

The first divertor DITE MK1A required very high current density, thus high power consumption and forces, which were considered to be unsolved problems. The DITE divertor was the first of a kind for testing the principle and hence was not an optimum design. It was demonstrated at Westinghouse that these problems could be solved with minor modification and a design of an integrated system has been given in detail. It was further proved that a simple multiple cascade T-shaped coil arrangement could reduce the ripple and current density drastically [2], thus improving the confinement and increasing available shielding space. A schematic picture of the cascade T-shaped divertor coil configuration and a diagram of the magnetic configuration produced by two T-shaped coils are shown in Fig. A.1. The improvement of ripple is shown in Fig. A.2. The ripple for the T-shaped coils lies within the shaded area. The magnetic flux surface is shown in Fig. A.3. The magnetic surfaces exhibit magnetic islands but are not ergodic for multiple T coils.

The INTOR TF coil system with 12 TF coils was used as a baseline for this calculation. The divertor fits between the gaps of two adjacent TF coils. The key reactor parameters are listed in Table A.1. The trace of null points for the DITE divertor is concave toward the divertor whereas it is a straight line or even concave toward the plasma for this new cascade T-shaped divertor. Therefore, the acceptance angle is larger than previous designs. It is estimated to be about 18°. The thermal conductivity for a number of cases were calculated by a Monte Carlo particle orbit code. Some particles launched in the ripple will be detrapped by drifting upward out of the region, and some will be detrapped due to collision. Typical detrapping effects are illustrated by the variation of the phase angles ($\xi = v_{\parallel}/v$) as a function of time in Fig. A.4. The phase angle oscillates rapidly when the particle is trapped inside the ripple. The period of oscillation of the phase angle is much larger for circulating and banana orbits. Figure A.4 shows particles launched in the ripple that are detrapped (a) without collision; and (b) due to collision. Many trappings and detrappings occur along the particle orbit, thereby justifying the diffusive model of transport. The

thermal conductivity for the divertor at three different locations is shown in Fig. A.5. Preliminary estimates are that thermal conductivity is enhanced by about a factor of 25 over axisymmetric neoclassical conductivity.

One and two dimensional neutronic calculations have been carried out. The best shielding material found was a composite of tungsten and borated water (90% W + 10% H_2 O (B)). The neutron flux attenuation rate as a function of thickness is shown in Fig. A.6. There are more than four decades of attenuation for a thickness of 60 cm of shielding space. The life time for a wall loading of 1 MW yr/m^2 would be 100 years for an optimistic dose limit of 10^9 Grays for an organic insulation or G-10, and at least 1 year for a conservative dose limit of 10^7 Grays.

The trimetric view of the divertor assembly is shown in Fig. 7. There is enough space in front of the central leg for blanket and shielding. Therefore, a part of the neutron energy can be recovered. A monolithic divertor assembly construction is shown in Fig. 8. The forces are transmitted to the TF coils through the two horizontal bars and heat stations which are specially designed to minimize the heat leakage and disconnection time. The bars are keyed to the divertor casing and attached to the heat station by cylindrical bearings. The divertor assembly can be freed and extracted simply by lifting up and dropping down the bars.

The characteristics of this advanced bundle divertor can be summarized as follows:

1. The ripple has been reduced to extremely low levels without sacrificing engineering requirements.

2. The particle confinement is improved and the magnetic surfaces are not ergodic.

3. The overall current density of the divertor coil is less than 4 kAmp/cm^2. The coil can be superconducting and the power requirement is minimal.

4. There is at least 60 cm of shielding space in front of the divertor. This gives four decades of attenuation of neutron dosage.

5. The monolithic divertor assembly design modular unit can be easily extracted for service or replacement with another module.

Key Parameters for a Reactor with a Bundle Divertor
(INTOR Baseline)

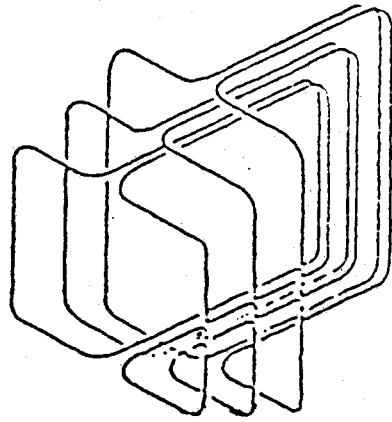|	INTOR
Bo (Tesla)	5.2
Ro (m)	5.4
A (m)	1.6
I_D (MA-turns)	19.2
J_D(kAmp/cm^2)	3.8
(per Tesla)	0.75
Coil cross section	2500
area (cm^2)	
D (m)	1.00
Shielding (m)	.60

Fig. A.1a   The trimetric view of a cascade T-shaped
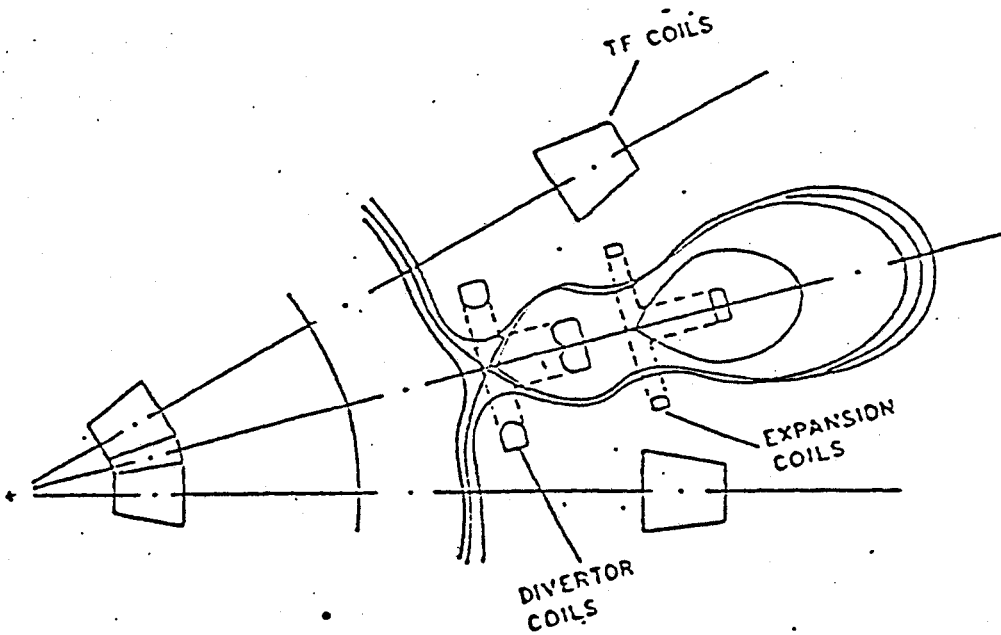   divertor coil configuration.

Fig. A.1b   The toroidal flux configuration for a two
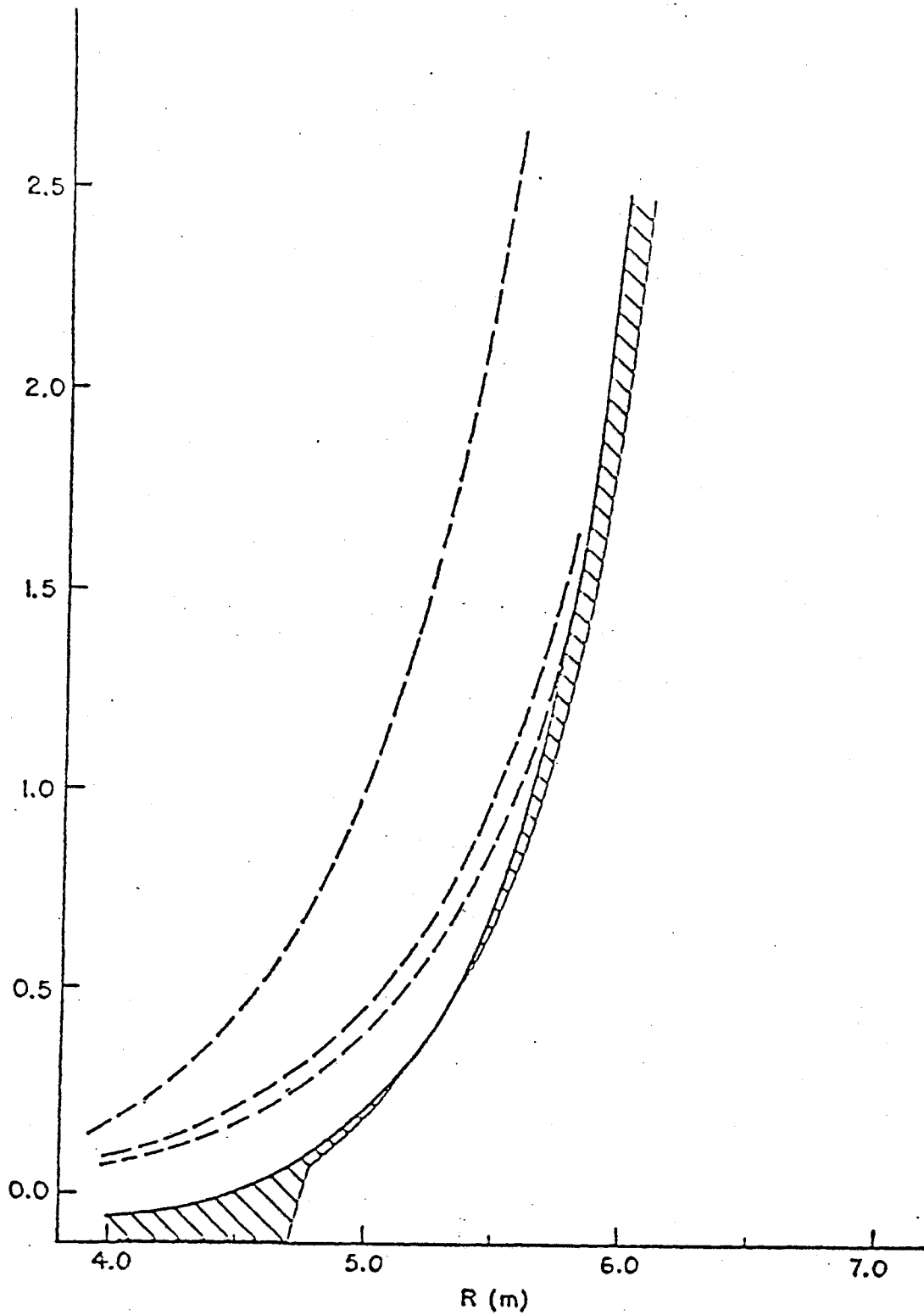   T-shaped coil divertor.

Fig. A.2   Divertor ripple on axis for the configurations
studied. The ripple for single "T" and cascade
are the lowest. They all fall within the shaded
region.
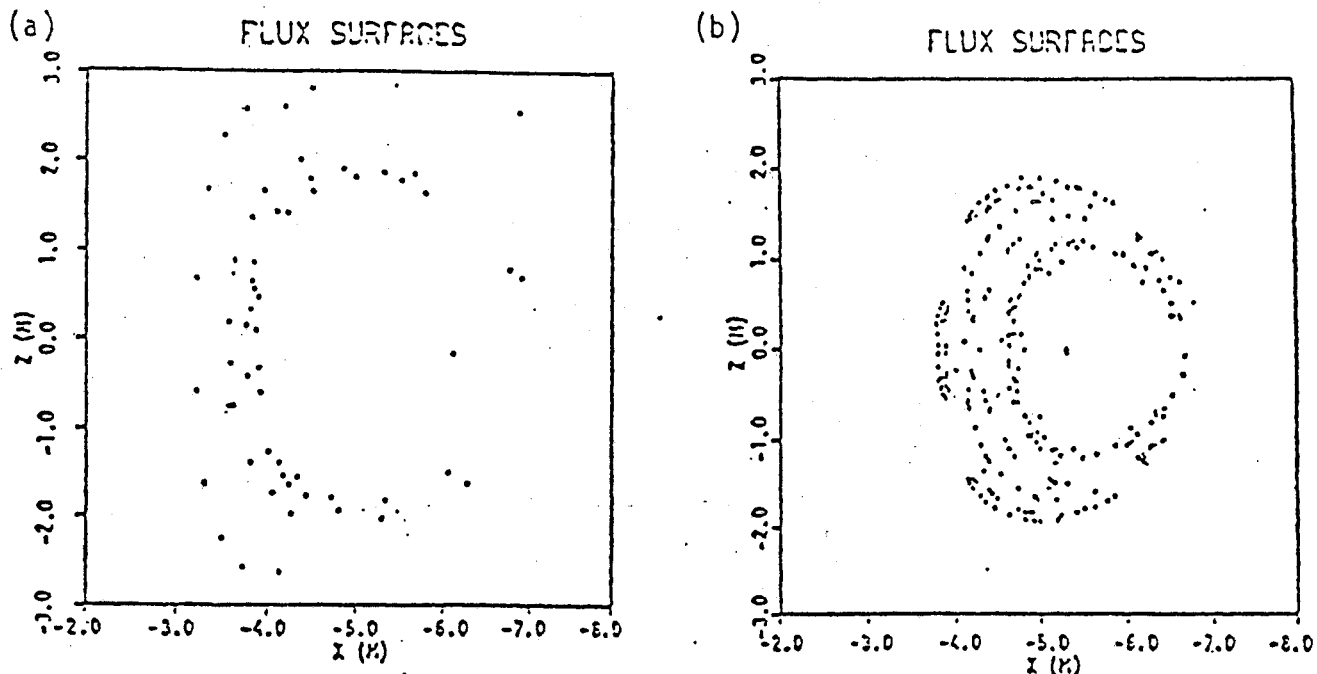
26

(a)

FLUX SURFACES

(b)

FLUX SURFACES

Fig. A.3 Magnetic surfaces of a tokamak with a T-shaped bundle divertor. (a) Surfaces are ergodic for one T coil. (b) Surfaces exhibit island structure for multiple T coils.
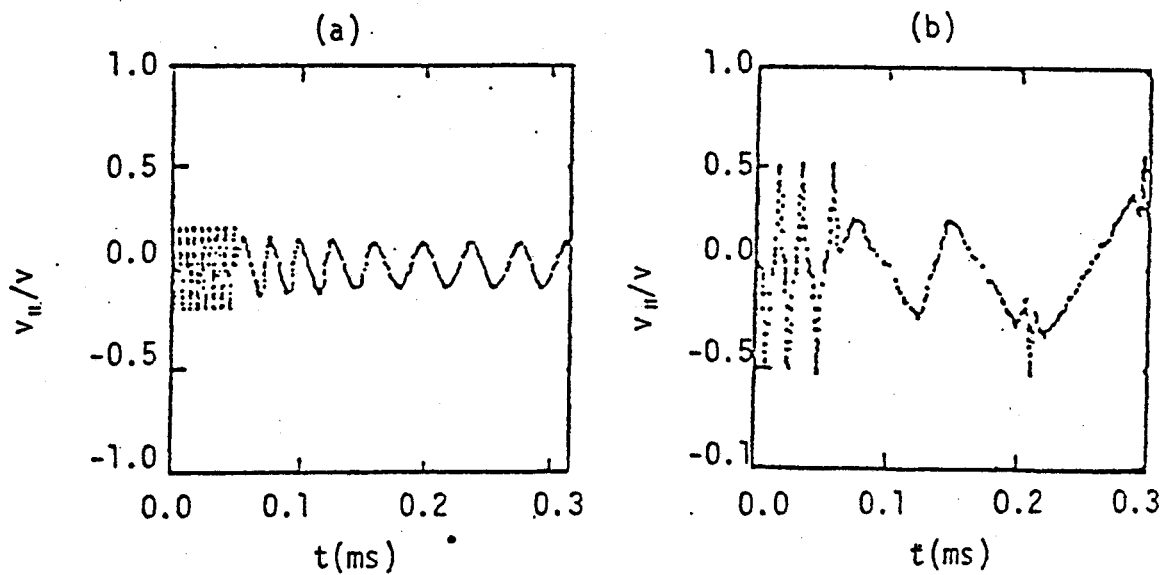
(a)

(b)

Fig. A.4 The variations of a phase angle as a function of time (a) without collision; (b) with collision.
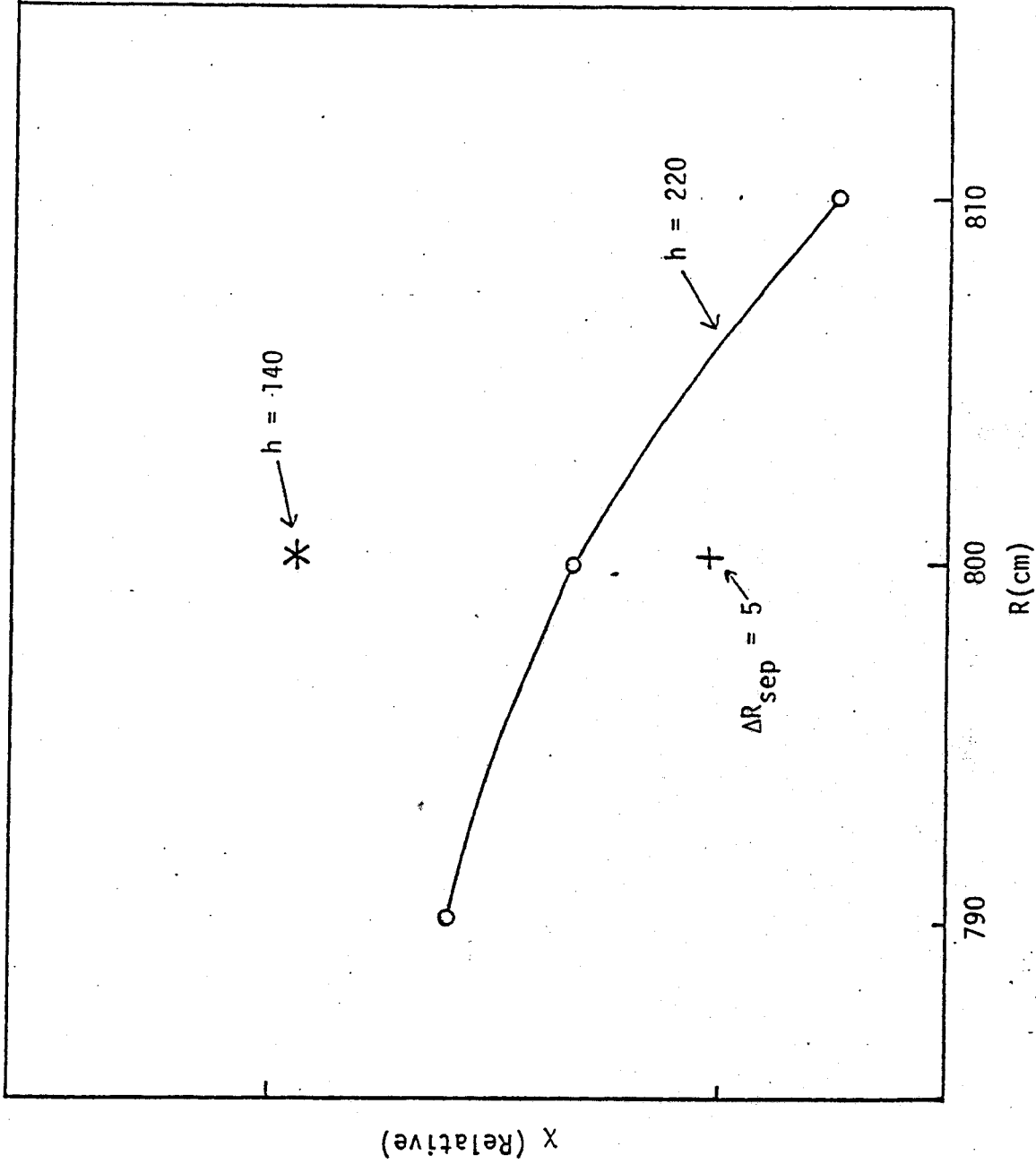
Fig. A.5   Relative thermal conductivity of a tokamak with a bundle divertor vs. radial position and height of the divertor. ΔR_{sep} is the separatrix from the axisymmetric plasma boundary.
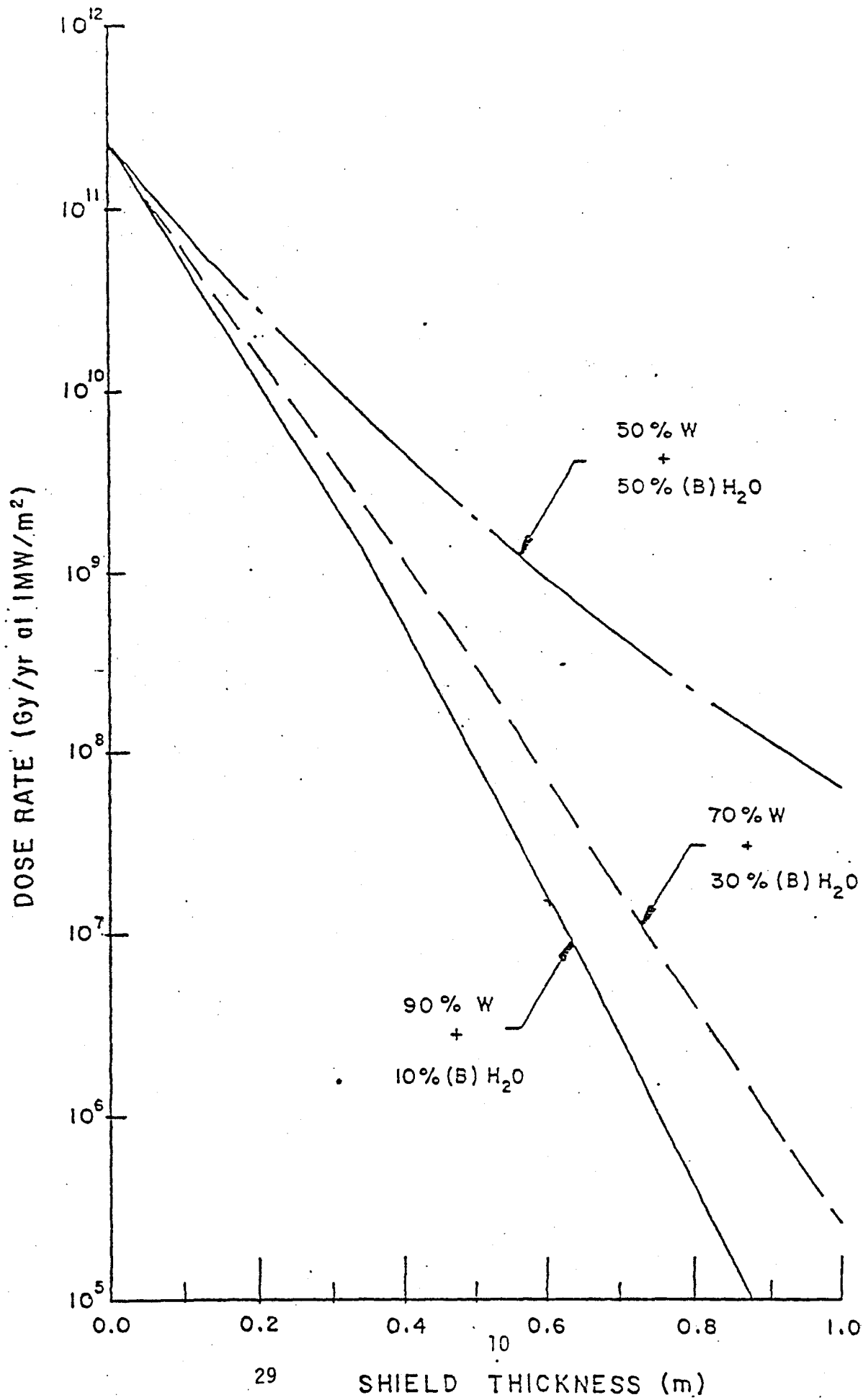
Fig. A.6 Dose rate as function of shield thickness. There is more than 4 decades of attenuation.
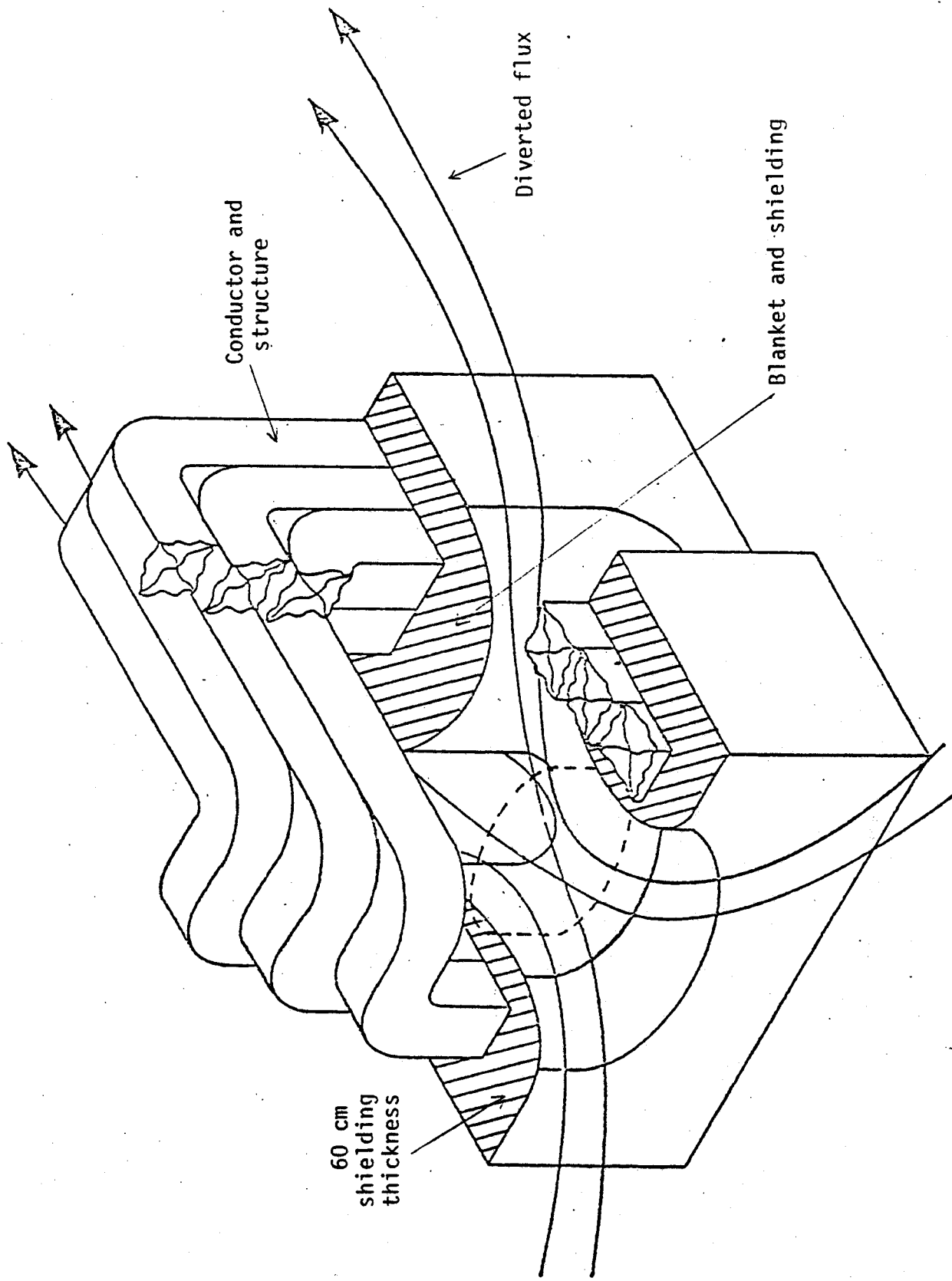
Fig. A.7   A trimetric view of a monolithic cascade T-shaped bundle divertor.[1] The shielding spaces are indicated by the shaded areas.

Diverted flux

Conductor and structure

Blanket and shielding

60 cm shielding thickness

ETF
BUNDLE
DIVERTOR

TF COIL

EXPANSION
COIL

DIVERTOR
CONTAINMENT
STRUCTURE
(MONOLITHIC CRATE)

TF COIL

COMPRESSIVE
SUPPORT

JET-MIT

RADIAL
RESTRAINT
BEAM

DIVERTOR
COIL

Fig. A.8 INTOR and FED bundle divertor assembly. An engineering
picture of an extractable monolithic structural design.

REFERENCES

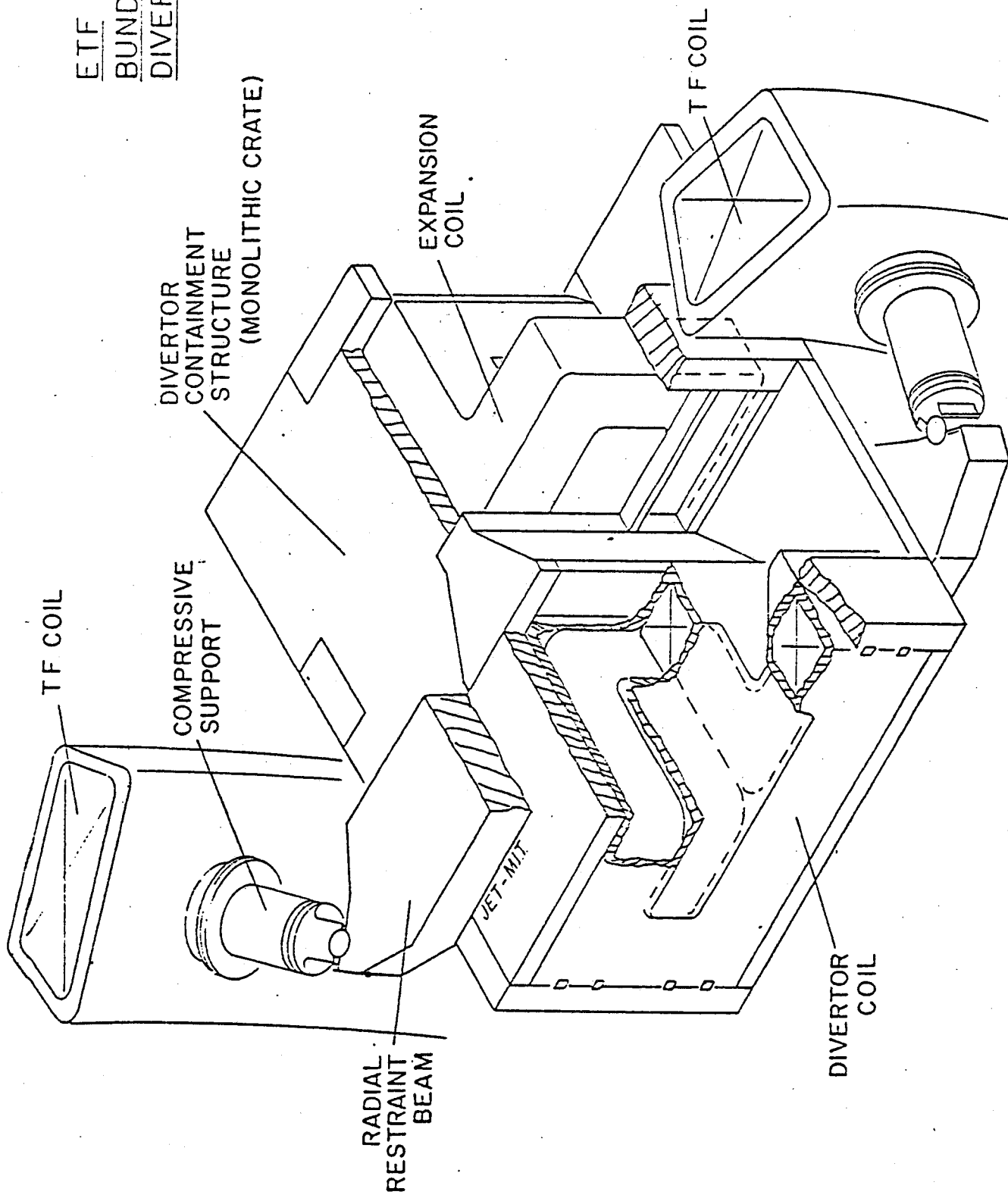[1] Technical Data I, Julich, Germany, March 1980.

[2] Yang, T. F., et al., MIT PFC/JA-81-4 (1981).

[3] Stott, P. E., Wilson, C. M., Gibson, A., "The Bundle Divertor-Part I; Magnetic Configuration", Nuclear Fusion 17 #3 (1977) 481.

[4] Wooton, Private Communication, February 1982.

[5] Bateman, G., et al., "Bundle Divertor Assessment for INTOR/FED", March 1982.

[6] Yang, T. F., Lee, A. Y., Ruck, G. W., Prevenslik, T., Smeltzer, B., "Design of an Advanced Bundle Divertor for the Demonstration Tokamak Hybrid Reactors", Proc. of the 8th IEEE Symp. on Engr. Probl. of Fusion Research 1 (1979) 615.

AEB, Plasma Physics Div., South Africa, De Villiers, Johan
AMPC Inc., Guest, Dr. F.
Association Euratom - CEA, Dept. de Physique de Plasma et de
      la Fusion Controle, France
Association Euratom - CEA, France, Brifford, Dr. G.
Associazione CNR-EURATOM, Italy, Ortolani, S.
Austin Research Associates
Australian National University, Hamberger, S.M.
Bank of Tokyo, Ltd., Japan, Azuma, Mr. Katsuhiko
Brookhaven National Laboratory, Powell, James R.
CNEN - Centro Frascati, Italy
Chalmers Univ. of Tech., Sweden, Wilhelmsson, K.H.B.
College of William and Mary, Montgomery, Prof. D.
Consoli, T., France
Cornell University, Fleischmann, Prof. H.
Cornell University, Laboratory for Plasma Studies
Culham Laboratory, United Kingdom
Dewar, R.L., New Jersey
Div. of Research and Labs., Austria, Frolov, V.
Ecole Royale Militaire, Belgium, Vandenplas, P.E.
EG&G Idaho, Inc., Crocker, Mr. J.
Electrical Power Research Institute, Amheard, Dr. Noel
FOM-Institute for Plasma Physics, Netherlands
General Atomic Company
Georgia Institute of Technology, Stacey, Jr., Dr. W.M.
Hiroshima University, Japan, Nishikawa, Prof. K.
ITT, India, Tewari, Prof. D.P.
I.V. Kurchatov Institute of Atomic Energy, USSR
INESCO, Inc., Wagner, Dr. C.
Institut fur Plasmaphysik, KFA Julich, FRG
Inst. Nacional de Invest. Nucleares, Mexico, Salas, J.S. Ramos
Japan Atomic Energy Res. Inst., Japan, Mori, Dr. S.
JET Joint Undertaking, United Kingdom
KFKI, Hungary, Kostka, P.
Kharkov Physical-Technical Institute, USSR, Tolok, Dr. V.T.
Kurchatov Institute, USSR, Eliseev, Dr. G.A.
Kyoto University, Japan, Uo, Prof. K.
Lawrence Berkeley Laboratory
Lawrence Livermore Lab, Magnetic Fusion Energy Div.
Lebedev Institute of Physics, USSR, Rabinovich, M.S.
Lockheed Palo Alto Research Lab, CA, Siambis, John
Los Alasmos Scientific Laboratory, CTR Division
Max-Planck-Institute fur Plasmaphysik, FRG
Nagoya University, Japan
National University of Singapore, Singapore
Naval Research Laboratory, Plasma Physics Division
Naval Surface Weapons Center, Uhm, Prof. Han S.
New York University, Courant Inst. of Math. Sci.
Nuclear Research Institute, Czechoslovakia, Bartosek, V.
Nuclear Service Corporation, Naymark, Mr. Sherman
Oak Ridge National Laboratory, Fusion Energy Division
Osaka University, Japan, Ito, H.
Palumbo, D., Belgium,
Physics International Group, Benford, Dr. Jim
Princeton University, Plasma Physics Laboratory
Rijksuniversiteit Gent, Belgium, Verheest, F.

Riso National Laboratory, Denmark, Jensen, V.O.
Royal Institute of Technology, Sweden, Lehnert, B.P.
Ruhr-Universitat,FRG, Kunze, H.J.
S. Kalinski Inst. of Plasma Phys. and Laser Microfusion,
      Poland, Fiedorowicz, H.
Sandia Research Laboratories, Plasma Physics Division
Science Applications, Inc., CO, Aamodt, Dr. Richard
Science Applications, Inc., MD, Dean, Dr. Stephen
Science Applications, Inc., CA
Science Applications, Inc., VA, Drobot, Dr. Adam
Science Council of Japan, Japan, Fushimi, K.
Siberian Section of the USSR Academy of Sciences, USSR
Soreq Nuclear Research Center, Israel, Rosenblum, M.
Stanford University, Buneman, Prof. O.
Technion, Israel, Rosenau, P.
Tel-Aviv University, Israel, Cuperman, S.
Tohoku University, Japan, Nagao, Prof. S.
TRW Defense and Space Systems, CA
U.S. Dept. of Energy, Office of Fusion Energy
U.S. Dept. of Energy, Kostoff, Dr. Ronald N.
U.S. Dept. of Energy, Thomasson, Dr. Neil
U.S. Dept. of Energy, Trivelpiece, Dr. A.W.
Universitat Innsbruck, Austria, Cap, F.
Universitat Stuttgart, FRG, Wilhelm, R.
Universite de Montreal, Canada, Paquette, G.
Universite Libre de Bruxelles, Belgium, Balescu, R.C.
University of Alberta, Canada, Offenberger, A.A.
University of B.C., Canada, Curzon, Dr. F.
University of California at Berkeley:
      Dept. of Electrical Eng. & Computer Sci.
      Dept. of Physics
University of California at Irvine, Dept. of Physics
University of California at L.A.:
      Dept. of Electrical Eng.
      Dept. of Physics
      Tokamak Fusion Lab.
University of California at L.A., Conn, Dr. Robert W.
University of California at L.A., Kastenberg, William E.
Univerisity of California at San Diego, Dept. of Physics
University of Illinois, Choi, Prof. Chan
University of Malay, Malaysia, Lee, S.
Univ. of Maryland:
      Dept. of Elec. Eng.
      Dept. of Physics
      Inst. for Phys. Sci. and Tech.
University of Michigan, Getty, Prof. Ward D.
University of Nairobi, Kenya, Malo, J.O.
University of Natal, South Africa, Hellberg, M.A.
University of Rochester, Simon, Prof. Albert
University of Saskatchewan, Canada, Hirose, A.
University of Texas:
      Center for Energy Studies
      Dept. of Physics
      Fusion Research Center
University of Tokyo, Japan, Uchida, Prof. T.
University of Tsukuba, Japan, Inutake, M.

University of Waikato, New Zealand, Hosking, R.J.
University of Washington, Sanders, R.
University of Washington, Vlases, Dr. George
University of Wisconsin:
    Dept. of Physics
    Dept. of Nuclear Eng.
University of Wisconsin, Tataronis, Dr. J.
Varien
Warsaw University Branch, Poland, Brzosko, J.S.
Yale University, Dept. of Applied Science

PFC BASE MAILING LIST

Argonne National Laboratory, TIS, Reports Section
Associazione EURATOM · CNEN Fusione, Italy, The Librarian
Battelle-Pacific Northwest Laboratory, Technical Info Center
Brookhaven National Laboratory, Research Library
Central Research Institute for Physics, Hungary, Preprint Library
Chinese Academy of Sciences, China, The Library
The Flinders University of S.A., Australia, Jones, Prof. I.R.
General Atomic Co., Library
General Atomic Co., Overskei, Dr. D.
International Atomic Energy Agency, Austria,
Israel Atomic Energy Commission, Soreq Nucl. Res. Ctr., Israel
Kernforschungsanlage Julich, FRG, Zentralbibliothek
Kyushu University, Japan, Library
Lawrence Berkeley Laboratory, Library
Lawrence Livermore Laboary, Technical Info. Center
Max-Planck-Institut fur Plasma Physik, FRG, Main Library
Nagoya University, Institute of Plasma Physics, Japan
Oak Ridge National Laboratory, Fusion Energy Div. Library
Oak Ridge National Laboratory, Derby, Roger
Physical Research Laboratory, India, Sen, Dr. Abhijit
Princeton University, PPL Library
Rensselaer Polytechnic Institute, Plasma Dynamics Lab.
South African Atomic Energy Board, S. Africa, Hayzen, Dr. A.
UKAEA, Culham Laboratory, England, Librarian
US Department of Energy, DOE Library
Universite de Montreal, Lab. de Physique des Plasmas, Canada
University of Innsbruck, Inst. of Theoretical Physics, Austria
University of Saskatchewan, Plasma Physics Lab., Canada
University of Sydney, Wills Plasma Physics Dept., Australia
University of Texas at Austin, Fusion Res. Ctr., Library
University of Wisconsin, Nucl. Eng. Dept., UW Fusion Library

INTERNAL MAILINGS

MIT Libraries
Industrial Liaison Office
G. Bekefi, A. Bers, D. Cohn, B. Coppi, R.C. Davidson,
T. Dupree, S. Foner, J. Freidberg, M.O. Hoenig, M. Kazimi,
L. Lidsky, E. Marmar, J. McCune, J. Meyer, D.B. Montgomery,
J. Moses, D. Pappas, R.R. Parker, N.T. Pierce, P. Politzer,
M. Porkolab, R. Post, H. Praddaude, D. Rose, J.C. Rose,
R.M. Rose, B.B. Schwartz, L.D. Smullin, R. Temkin, P. Wolff,
T-F. Yang

2